



Providing Choice & Value
Generic CT and MRI Contrast Agents

**FRESENIUS
KABI**

CONTACT REP

AJNR

Arterial Spin-Labeling in the Assessment of Pediatric Nontraumatic Orbital Lesions

S. Neumane, A. Lesage, V. Dangouloff-Ros, R. Levy, C.-J. Roux, M.P. Robert, D. Bremond-Gignac and N. Boddaert






AJNR Am J Neuroradiol 2023, 44 (10) 1219-1223

doi: <https://doi.org/10.3174/ajnr.A7977>

<http://www.ajnr.org/content/44/10/1219>

This information is current as
of July 17, 2025.

Arterial Spin-Labeling in the Assessment of Pediatric Nontraumatic Orbital Lesions

 S. Neumane, A. Lesage,  V. Dangouloff-Ros, R. Levy,  C.-J. Roux, M.P. Robert,  D. Bremond-Gignac, and  N. Boddaert



ABSTRACT

SUMMARY: Benign and malignant pediatric orbital lesions can sometimes have overlapping features on conventional MR imaging sequences. MR imaging of 27 children was retrospectively reviewed to describe the signal of some common pediatric extraocular orbital lesions on arterial spin-labeling and to evaluate whether this sequence helps to discriminate malignant from benign masses, with or without ADC value measurements. Qualitative and quantitative assessments of arterial spin-labeling CBF and ADC were performed. All lesions were classified into 3 arterial spin-labeling perfusion patterns: homogeneous hypoperfusion (pattern 1, $n = 15$; benign lesions), heterogeneous hyperperfusion (pattern 2, $n = 9$; cellulitis, histiocytosis, malignant tumors), and homogeneous intense hyperperfusion (pattern 3, $n = 3$; infantile hemangiomas). Arterial spin-labeling can be a valuable tool to improve the diagnostic confidence of some orbital lesions, including infantile hemangioma. An algorithm is proposed.

ABBREVIATIONS: ASL = arterial spin-labeling; av = averaged; IH = infantile hemangioma; LBF = lesion blood flow; OL = orbital lesion; ONG = optic nerve glioma; rLBF = relative lesion blood flow; RMS = rhabdomyosarcoma

A wide variety of benign and malignant lesions can present in the orbital region, ranging from developmental anomalies to infectious processes and malignancies. Imaging is essential for their evaluation and to guide intervention, and MR imaging is the main technique used in children. Many pediatric orbital lesions (OLs) have a distinct appearance on conventional sequences, but benign and malignant processes can have a similar appearance. DWI and ADC values have been increasingly used to characterize OLs. Several studies found relevant differences between benign and malignant lesions, but with a different range of reported sensitivities, specificities, and optimal threshold ADC values for distinguishing between lesions.¹⁻⁴

MR imaging perfusion is increasingly used in the evaluation of head and neck anomalies and cerebral tumors,⁵⁻⁷ but few studies describe its potential use in the evaluation of OLs. Some studies showed that the combination of DWI and dynamic contrast-enhanced MR imaging considerably improved the specificity and sensitivity for differentiating radiologically indeterminate malignant from benign orbital masses.^{8,9} Arterial spin-labeling (ASL) is a noninvasive MR imaging perfusion technique that provides measurements reflecting the degree of lesion angiogenesis and vascular density.⁵ Its role in the characterization of OLs in children has not been studied yet. ASL tumor blood flow and ADC values (alone and in combination) have been shown to be useful in differentiating orbital lymphoma from idiopathic inflammatory pseudotumor in an adult cohort.⁹

The purpose of this study was to describe the ASL signal of some common pediatric extraocular OLs and to evaluate its relevance in discriminating malignant from benign masses, with or without ADC value measurements.

MATERIALS AND METHODS

Study Design and Subjects

This retrospective descriptive study included 27 children (mean age, 4.2 [SD, 4.3] years; range, 0.2–15.0 years) referred to Necker-Enfants Malades University Hospital between January 2015 and September 2022, who underwent MR imaging for evaluation of a nontraumatic extraocular OL with a routine protocol including ASL perfusion. Patients without a confirmed diagnosis were

Received March 8, 2023; accepted after revision August 2.

From the Departments of Pediatric Radiology (S.N., A.L., V.D.-R., R.L., C.-J.R., N.B.) and Ophthalmology (M.P.R., D.B.-G.), Hôpital Universitaire Necker Enfants Malades, Assistance Publique–Hôpitaux de Paris, Université Paris Cité, Paris, France; NeuroSpin, UNIACT (S.N.), Commissariat à l'Énergie Atomique et aux Énergies Alternatives (CEA), Université Paris-Saclay, Gif-sur-Yvette, France; Department of Pediatric Radiology (A.L.), Centre Hospitalier Universitaire Saint-Justine, Montréal, Quebec, Canada; Institut Imagine (V.D.-R., R.L., C.-J.R., N.B.), Institut National de la Santé et de la Recherche Médicale (INSERM) U1163 and U1299, Université Paris Cité, Paris, France; Centre Borelli UMR 9010 (M.P.R.), Université Paris Cité, Université Paris-Saclay, ENS Paris-Saclay, CNRS, SSA, Institut National de la Santé et de la Recherche Médicale (INSERM), Paris, France; and Team 17 (D.B.-G.), Institut National de la Santé et de la Recherche Médicale, UMR5138, Université Paris Cité, Paris, France.

Please address correspondence to Nathalie Boddaert, MD, PhD, Pediatric Radiology Department, Hôpital Universitaire Necker Enfants Malades, AP-HP, Université Paris Cité, F-75015, Paris, France; e-mail: nathalie.boddaert@aphp.fr

 Indicates article with online supplemental data.

<http://dx.doi.org/10.3174/ajnr.A7977>

excluded. Initial symptoms and final diagnoses were obtained from the electronic medical record. Approval was obtained from the institutional ethics board (CRM-2301-324). According to local regulations, consent was waived for this retrospective analysis of anonymized data. This study was recorded in the general register of the Assistance Publique-Hôpitaux de Paris in January 2023 (No. 2023 0126171431).

MR Imaging Acquisition

An ASL perfusion sequence was acquired on a 1.5T or 3T MR imaging scanner (Signa HDxt; GE Healthcare) and consisted of a concurrent spiral 3D pseudocontinuous ASL (12-channel head coil; 3D volume with a 4-mm section thickness using a fast spin-echo acquisition [TR/TE = 4453/10.96 ms; number of axial slices = 40; resolution in plane = 1.875×1.875 mm; postlabeling delay = 1025 ms; flip angle = 155°]). All patients underwent a routine MR imaging examination, including T1 and T2 sequences with additional sequences performed at the discretion of the attending radiologist (gadolinium injection, DWI), depending on the indications.

MR Imaging: Qualitative and Quantitative Analysis

All the cases were reviewed in radio-ophthalmology staff meetings. MR imaging data were retrospectively reviewed in consensus by S.N. and a senior pediatric neuroradiologist, R.L.

ASL. Qualitative assessment of CBF maps was made by coregistration with conventional sequences to describe the signal intensity of individual lesions (hyperintense, warm colors; isointense and hypointense, cold colors) and homogeneity. Lesion blood flow (LBF) measurements (in milliliters/minute/100 g of tissue) were obtained using dedicated postprocessing software on Advantage Windows workstations (GE Healthcare). Freehand ROIs were placed on a minimum of 3 axial plans over the most representative area for small or homogeneous lesions and over the maximal and minimal signal areas of large or heterogeneous masses. Measurements were averaged (av) (LBFav) for each lesion. To take into account general signal variations between subjects and facilitate comparison with other studies, we calculated the relative LBF (rLBF) or lesion-to-cortex signal ratio by comparing the LBFav of each lesion with the average CBF obtained by freehand ROIs drawn over the ipsilateral temporal cortex ($\text{CBF}_{\text{av, cortex}}$) ($\text{rLBF} = \text{LBFav}/\text{CBF}_{\text{av, cortex}}$).

DWI-ADC. The ADC maps were processed in a manner comparable with ASL maps, using similar manual ROIs and similar averaging ($\text{ADC}_{\text{av, lesion}}$ and $\text{ADC}_{\text{av, cortex}}$), and lesion-to-cortex ADC ratios ($\text{rADC} = \text{ADC}_{\text{av, lesion}}/\text{ADC}_{\text{av, cortex}}$) were calculated.

Data Analysis. Statistical analyses were performed using R 3.3.3 statistical and computing software (<http://www.r-project.org/>). Results are presented as medians and ranges in the text. Quantitative rLBF data were compared among the 3 patterns using 1-way ANOVA.

RESULTS

We analyzed 27 OLs, including 23 benign lesions (vascular [$n=9$] and nonvascular [$n=9$] masses, infectious processes [$n=3$], optic nerve glioma [ONG] [$n=2$]) and 4 malignant

tumors (rhabdomyosarcomas [RMS, $n=2$], metastatic retinoblastoma [$n=1$], and metastatic neuroblastoma [$n=1$]), with histopathologic evidence available for most cases requiring confirmation other than clinical or radiologic (Online Supplemental Data).

ASL

Qualitative and quantitative assessment of ASL maps showed 3 significantly distinct profiles ($F_{(2, 24)} = 86.44$; $P < .001$): pattern 1, homogeneous hypoperfusion ($n=15$); pattern 2, heterogeneous hyperperfusion ($n=9$); and pattern 3, homogeneous intense hyperperfusion ($n=3$) (Online Supplemental Data and Fig 1). Pattern 1 comprised benign OLs, including lymphatic malformation dermoid cysts, dacryops, fibrolipoma, and ONG, with median rLBF = 0.44 (range, 0.21–0.63). On the opposite side of the spectrum, pattern 3 was characteristic of infantile hemangiomas (IHs), with a median rLBF = 10.43 (range, 9.56–18.73). Pattern 2 (median rLBF = 1.23; range, 0.91–2.91) included orbital cellulitis, histiocytosis, and malignant neoplasms with overlapping rLBF (median = 2.75; range, 1.0–2.91; median = 1.07; range, 0.91–1.23; and median = 1.54; range, 1.14–1.88, respectively). There was no overlap between the rLBF range of pattern 3 and that of other groups. Most (78%) benign OLs presented as homogeneous ASL perfusion (patterns 1 and 3), while all malignant tumors were heterogeneous (pattern 2).

DWI-ADC

DWI was available in 78% of cases ($n=21$) (Online Supplemental Data and Fig 2), among which ADC values were decreased in all malignant tumors (median ADC = $0.85 \times 10^{-3} \text{ mm}^2/\text{s}$), abscessed portions of infectious processes (median ADC = $0.77 \times 10^{-3} \text{ mm}^2/\text{s}$), dermoid cysts (median ADC = $0.65 \times 10^{-3} \text{ mm}^2/\text{s}$), and the non-Langerhans cell histiocytosis. ADC values were increased for all IHs (median ADC = $1.69 \times 10^{-3} \text{ mm}^2/\text{s}$), orbital cellulitis (median ADC = $2.20 \times 10^{-3} \text{ mm}^2/\text{s}$), lymphatic malformations (median ADC = $2.60 \times 10^{-3} \text{ mm}^2/\text{s}$), and cases of dacryops, fibrolipoma, and Langerhans cell histiocytosis.

DISCUSSION

Pediatric orbital masses are a heterogeneous group that can present with various and nonspecific manifestations. Clinical presentation and conventional imaging features do not always allow an accurate diagnosis. Given the substantial risk associated with orbital biopsies, additional predictors of the histologic nature of OLs are useful. We have found, in this case series, 3 distinct patterns on ASL maps that allow classifying all lesions: homogeneous hypoperfusion (pattern 1, including only benign lesions), heterogeneous hyperperfusion (pattern 2, including orbital infectious processes, histiocytosis, and malignant neoplasms), and homogeneous very intense hyperperfusion (pattern 3, characteristic of IHs, without rLBF values overlapping with those of other groups) (Figs 3 and 4).

Within pattern 2, there was an rLBF overlap among the OL subgroups, with ADC values refining the characterization of these lesions because ADC values were increased for orbital cellulitis, variable for histiocytosis, and decreased (diffusion restriction) for malignant tumors. Across the entire cohort, ADC values were decreased in malignant tumors, while increased in most benign

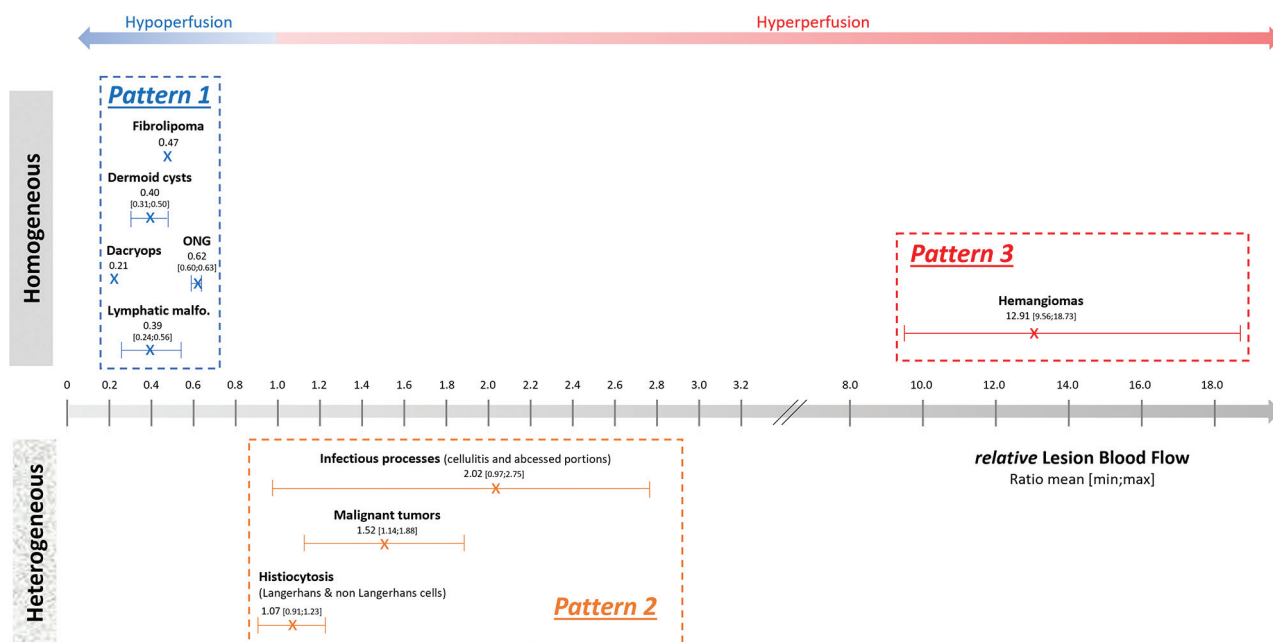


FIG 1. Representation of ASL perfusion profiles of the 27 OLs, according to their homogeneity and signal intensity. Mean rLBF and ranges by diagnostic subgroups show 3 significantly distinct profiles ($P = 1.08 \times 10^{-11}$): homogeneous hypoperfusion (pattern 1, blue), heterogeneous iso- or hyperperfusion (pattern 2, orange), and homogeneous hyperperfusion (pattern 3, red). rLBF corresponds to the ratio between LBF and CBF from the ipsilateral temporal cortex.

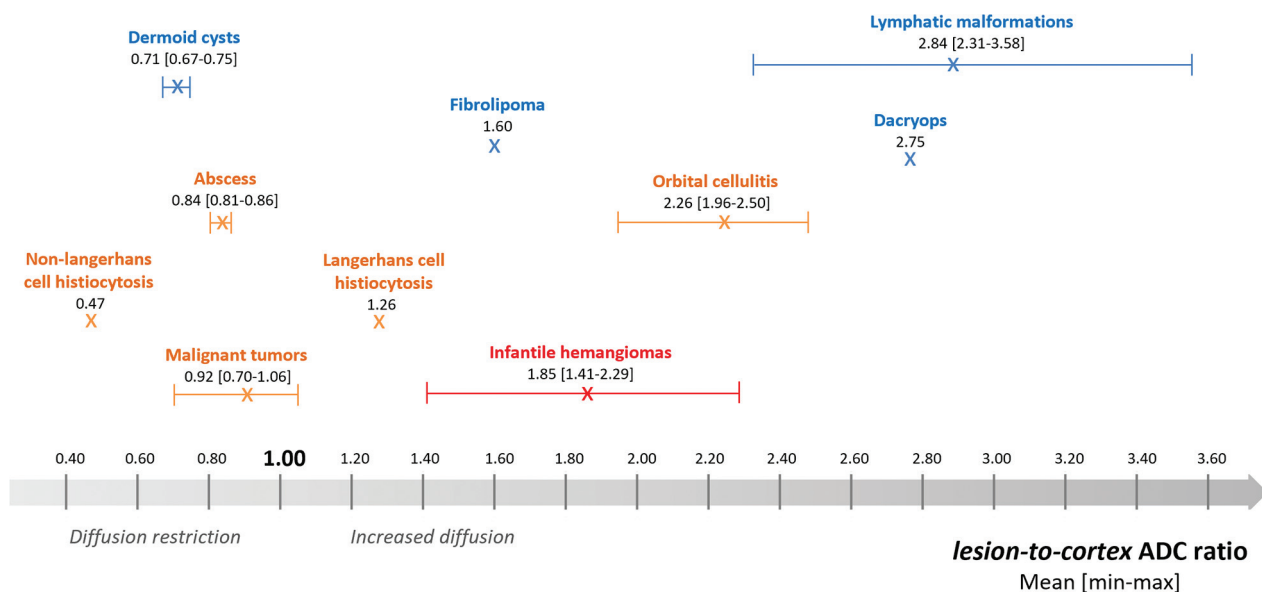


FIG 2. Distribution of ADC ratios ($n = 21$) by diagnostic subgroups. Lesion-to-cortex ADC ratios were calculated by dividing the lesion mean ADC by the ipsilateral temporal cortex mean ADC (both directly obtained for each patient by drawing an ellipsoid ROI over an area similar to that used for ASL measurements, taking care to avoid volume averaging with adjacent structures, particularly fat and bone). The distinct subportions of infectious processes (eg, abscessed areas with characteristic diffusion restriction and denser tissular inflammatory parts, cellulitis) were assessed separately. Colors correspond to the ASL perfusion profile groups presented in Fig 1 (pattern 1: blue; pattern 2: orange; pattern 3: red).

masses, in line with previous studies reporting lower ADC values in malignant orbital tumors than in benign orbital masses in adult^{1,10} and pediatric populations.^{3,4}

In agreement with previous studies,^{8,9,11} this work confirms the interest in using complementary diffusion and perfusion MR imaging techniques for characterizing orbital masses, while

suggesting that ASL might be more informative than ADC when it comes to differentiating benign vascular lesions from malignant tumors.

The specificity of pattern 3 is of particular interest. There can be an overlap between the imaging appearance of IHs and malignant tumors, mainly RMS,^{12,13} because they may have similar signal on

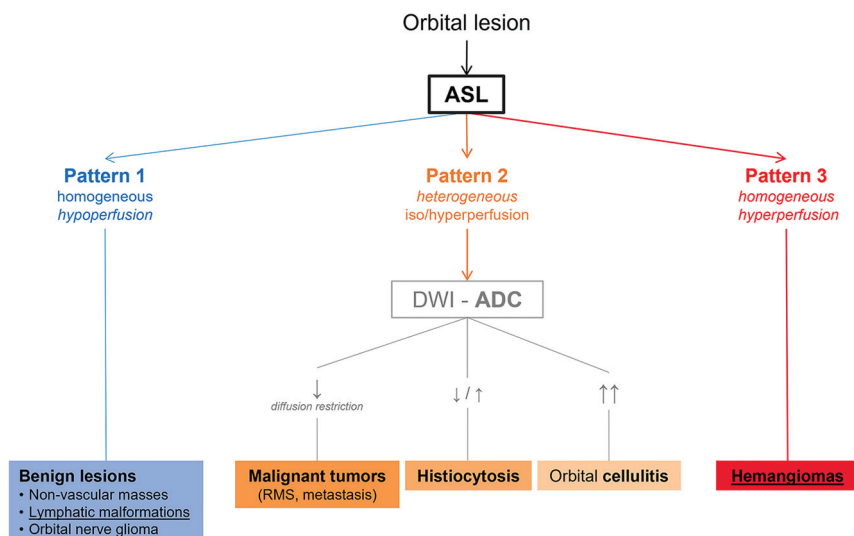


FIG 3. Summary algorithm for radiologic interpretation. There are 3 distinct patterns derived from ASL perfusion analysis: Pattern 1 (blue) corresponds to benign masses presenting homogeneous low lesion blood flow; pattern 2 (orange) describes heterogeneous iso- or hyperperfused lesions, including malignancies; pattern 3 (red) is characteristic of hemangiomas (benign vascular lesions), presenting specific homogeneous and very intense hyperperfusion. ADC assessment within pattern 2 contributed to differentiating malignant tumors (presenting diffusion restriction) from benign lesions like orbital cellulitis (with increased diffusion). Lymphatic malformations (pattern 1) and IHS (pattern 3), two frequent vascular anomalies (underlined) in pediatric population, presented with very distinct ASL perfusion homogeneous profiles.

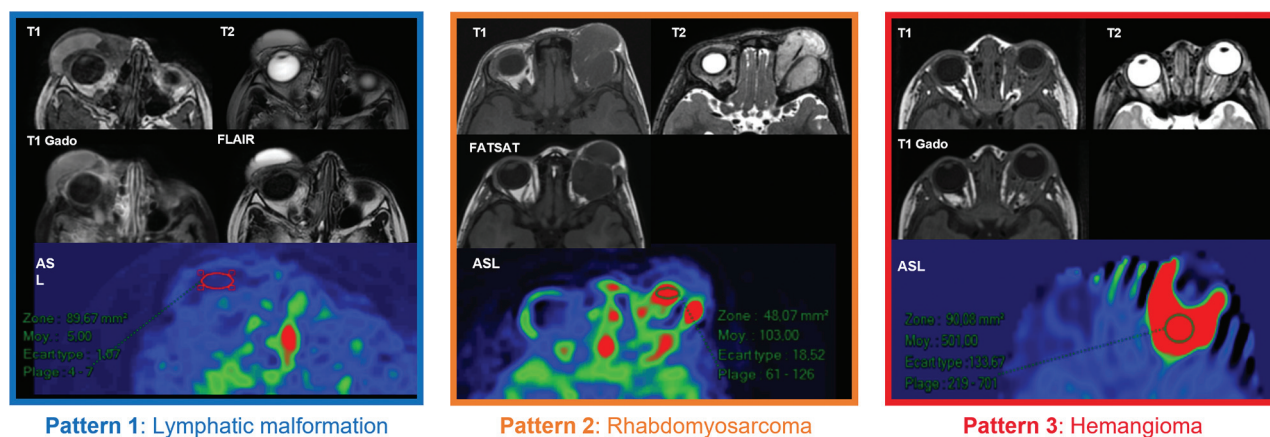


FIG 4. Conventional MR imaging sequences and ASL maps of representative patients for the 3 perfusion patterns. Pattern 1 (homogeneous hypoperfusion profile, characterized by cold dark colors on the CBF map over the lesion area): Lymphatic malformation, right vascular anomaly (patient 12, mean LBF = 10 mL/min/100g tissue, rLBF = 0.24). Pattern 2 (heterogeneous hyperperfusion profile, consisting of multiple bright color patches within the lesion area): Rhabdomyosarcoma, left malignant tumor (patient 24, mean LBF = 74 mL/min/100g tissue, rLBF = 1.84). Pattern 3 (homogeneous very intense hyperperfusion profile, corresponding to a uniform bright warm color area in the CBF maps): IH, left vascular anomaly (patient 16, mean LBF = 515 mL/min/100g tissue, rLBF = 18.73). Conventional sequences: T1 and T2 WI, T1 Gado (T1WI with gadolinium-based contrast medium), FLAIR, FATSAT (fat-suppression T1WI sequence).

T2WI and T1WI+C.^{12,14} IHS present earlier in life, are more often homogeneous on T1WI+C, are usually more hyperintense on T2WI than RMS, and commonly present with flow voids.^{13,14} They also have higher ADC values than RMS.¹² Adding ASL data may help with the differential diagnosis: in our cohort, all IHS (in the proliferating phase at the time of MR imaging) had a very distinct appearance, with homogeneous, very high perfusion signal (pattern 3), in accordance with what has been described in other cervicofacial locations.⁶ No other lesion presented an ASL signal as intense as that in IHS, including malignant tumors.

Moreover, IHS and lymphatic malformations, which are among the most frequent vascular anomalies of the pediatric

orbit, had very distinct ASL perfusion homogeneous profiles in our cohort (patterns 3 and 1, respectively).

ASL is a robust imaging sequence. It has a relatively rapid acquisition time and is noninvasive (does not require a venous access and the injection of exogenous contrast medium), 2 very valuable factors in the pediatric population. It has some limitations, including being sensitive to motion and susceptibility artifacts from metal and having a low SNR. The ASL sequence also has a limited spatial resolution, which makes it less useful in the evaluation of very small lesions.

We have chosen to present average LBF values (instead of maximal values), given that most of the analyzed lesions had a

homogeneous signal. In addition, the generally small size of OLs does not always allow calculating values for different lesion areas.

The main limitation of this study is the number and variety of cases, especially those with malignant tumors. Thus, despite the interesting categorization of pediatric OLs according to their ASL perfusion patterns, the proposed algorithm requires verification in larger cohorts that include a larger spectrum of OLs.

Despite these limitations, our descriptive study offers a novel framework of distinctive hemodynamic properties of some common pediatric OLs, proposing an algorithm that may contribute to the diagnostic orientation of OLs by combining, for the first time, ASL and DWI-ADC.

CONCLUSIONS

ASL perfusion-weighted MR imaging can be a valuable noninvasive tool to improve the discrimination among a full spectrum of benign and malignant orbital processes, by refining the short differential provided by the clinical presentation and conventional sequences. Especially, ASL may improve the diagnostic confidence of benign vascular lesions, in particular IHs requiring medical treatment. Furthermore, information provided by relevant orbital MR imaging is valuable for the oculoplastic surgeon for guiding an intervention. We hope to encourage other teams to integrate ASL into their routine orbital MR imaging protocols to explore its potential.

ACKNOWLEDGMENTS

We thank the children and their parents for their participation in this study.

Disclosure forms provided by the authors are available with the full text and PDF of this article at www.ajnr.org.

REFERENCES

1. Sepahdari AR, Politi LS, Aakalu VK, et al. Diffusion-weighted imaging of orbital masses: multi-institutional data support a 2-ADC threshold model to categorize lesions as benign, malignant, or indeterminate. *AJNR Am J Neuroradiol* 2014;35:170–75 [CrossRef Medline](#)
2. Sepahdari AR, Aakalu VK, Kapur R, et al. MRI of orbital cellulitis and orbital abscess: the role of diffusion-weighted imaging. *AJR Am J Roentgenol* 2009;193:W244–50 [CrossRef Medline](#)
3. Maldonado FR, Princich JP, Micheletti L, et al. Quantitative characterization of extraocular orbital lesions in children using diffusion-weighted imaging. *Pediatr Radiol* 2021;51:119–27 [CrossRef Medline](#)
4. Jaju A, Rychlik K, Ryan ME. MRI of pediatric orbital masses: role of quantitative diffusion-weighted imaging in differentiating benign from malignant lesions. *Clin Neuroradiol* 2020;30:615–24 [CrossRef Medline](#)
5. Dangouloff-Ros V, Deroulers C, Foissac F, et al. Arterial spin-labeling to predict brain tumor grading in children: correlations between histopathologic vascular density and perfusion MR imaging. *Radiology* 2016;281:553–66 [CrossRef Medline](#)
6. Boulouis G, Dangouloff-Ros V, Boccara O, et al. Arterial spin-labeling to discriminate pediatric cervicofacial soft-tissue vascular anomalies. *AJNR Am J Neuroradiol* 2017;38:633–38 [CrossRef Medline](#)
7. Mamlouk MD, Hess CP. Arterial spin-labeled perfusion for vascular anomalies in the pediatric head and neck. *Clin Imaging* 2016;40:1040–46 [CrossRef Medline](#)
8. Xu XQ, Qian W, Ma G, et al. Combined diffusion-weighted imaging and dynamic contrast-enhanced MRI for differentiating radiologically indeterminate malignant from benign orbital masses. *Clin Radiol* 2017;72:903.e9–903–15 [CrossRef Medline](#)
9. Ro SR, Asbach P, Siebert E, et al. Characterization of orbital masses by multiparametric MRI. *Eur J Radiol* 2016;85:324–36 [CrossRef Medline](#)
10. Razek AA, Elkharnay S, Mousa A. Differentiation between benign and malignant orbital tumors at 3-T diffusion MR-imaging. *Neuroradiology* 2011;53:517–22 [CrossRef Medline](#)
11. Eissa L, Abdel Razek AA, Helmy E. Arterial spin-labeling and diffusion-weighted MR imaging: utility in differentiating idiopathic orbital inflammatory pseudotumor from orbital lymphoma. *Clin Imaging* 2021;71:63–68 [CrossRef Medline](#)
12. Kralik SF, Haider KM, Lobo RR, et al. Orbital infantile hemangioma and rhabdomyosarcoma in children: differentiation using diffusion-weighted magnetic resonance imaging. *J AAPOS* 2018;22:27–31 [CrossRef Medline](#)
13. Sarioglu FC, Sarioglu O, Guleryuz H, et al. MRI-based texture analysis for differentiating pediatric craniofacial rhabdomyosarcoma from infantile hemangioma. *Eur Radiol* 2020;30:5227–36 [CrossRef Medline](#)
14. Lope LA, Hutcheson KA, Khademian ZP. Magnetic resonance imaging in the analysis of pediatric orbital tumors: utility of diffusion-weighted imaging. *J AAPOS* 2010;14:257–62 [CrossRef Medline](#)